

Performance comparison of graphene and graphene oxide-supported palladium nanoparticles as a highly efficient catalyst in oxygen reduction

Mir Reza Majidi, Seyran Ghaderi*

Department of Analytical Chemistry, Faculty of Chemistry, University of Tabriz, Tabriz, Iran

Received: 23 October 2016, Accepted: 18 April 2017, Published: 19 April 2017

Abstract

In this work, the performance of graphene nanosheets (GNs) and graphene oxide (GO) nanosheets, as a support for palladium nanoparticles (PdNPs) toward oxygen reduction reaction (ORR), was studied. The graphene nanosheets were functionalized by a new and simple method. The PdNPs were synthesized on a glassy carbon electrode (GCE) modified with GNs or GO *via* a potentiostatic method without using any templates, surfactants or stabilizers. The surface morphology of the modified electrodes was studied by scanning electron microscopy, energy dispersive X-ray and X-ray diffraction techniques. Cyclic voltammetry and rotating disk electrode (RDE) voltammetry methods were used for calculation of electrochemical parameters of the ORR. The GCE modified with PdNPs-GO exhibited a higher catalytic activity in comparison with PdNPs-GNs toward ORR. The high electrocatalytic activity of PdNPs-GO/GCE was attributed to oxygen-containing groups that were formed on the GO during functionalization of graphene nanosheets. These groups act as anchoring sites for metal nanoparticles and improve their dispersion on GO nanosheets. Also, mechanism of ORR was intensively investigated and transferred electron numbers in reaction was calculated using RDE data analysis. Finally, stability of the modified electrodes was studied and the results confirmed that the GCE modified with PdNPs-GO has a long-term stability.

Keywords: Oxygen reduction reaction; functionalization; graphene oxide nanosheets; palladium nanoparticles; electrodeposition.

Introduction

Oxygen reduction reaction has been extensively studied in recent years due to its importance in many fields, such as electrochemical energy conversion/storage, metal corrosion, and electrocatalysis [1-3]. It is one of the most important topics for the perception of highly effective fuel cells, batteries and other applications [4-7]. Since oxygen reduction has the sluggish kinetics that restricts large-

scale application of the fuel cells, tremendous research efforts have been focused on developing effective catalysts for ORR [8-9].

Up to now, platinum (Pt) has been known as the most efficient catalytic in fuel cell systems but, Pt is one of the most expensive metals. Therefore, researchers have focused on the other noble metals as catalyst to replace Pt [10]. Palladium is an appropriate alternative metal because

*Corresponding author: Seyran Ghaderi

Tel: +98 (41) 33393111, Fax: +98 (41) 33340191

E-mail: seyranghaderi@gmail.com

electrochemical properties of Pd like Pt and ORR have the same mechanism on these noble metals [11]. Also, Pd is less expensive and more abundant than Pt [12].

However, due to the relatively low reserves of Pd on earth, it is still too expensive for practical applications in fuel cell systems. Several studies have been performed to decrease Pd usage *via* various preparation methods of Pd nanoparticles [13,14]. Metal nanoparticles have properties largely different from their bulk counterpart, for example, superior catalytic performance, large surface-to-volume ratio and special binding sites available on the surface of the particles [15].

Electrodeposition is an efficient and controllable method to synthesize metal nanoparticles [16-18]. In this technique, no stabilizers and additives are used, therefore; this is an effective procedure to synthesis Pd nanoparticles with high density of atoms and clean surfaces. The electrodeposition process is a fast method and in this method, the obtained Pd particles are always tens of nanometers in size as reported previously [19].

Over the last years, Pd nanoparticles supported by high-area carbon are outstanding used in the preparation of highly active catalyst materials toward ORR [5, 20-22]. Several carbon-supported PdNPs have already been reported. Graphene nanosheets, as a new kind of two-dimensional carbon material consisting of a single or several atomic layers, have been attracted much interest due to the excellent electrical conductivity and large specific surface area.

The theoretical specific surface area of a graphene single-layer is much higher than traditional carbon materials [23,24].

But, graphene nanosheets tend to

form irreversible accumulates to form graphite through Van der Waals interactions, thus; the specific surface area of agglomerated GNs is 10 times smaller than GNs [25]. Also, when the metal ions are electrodeposited on GNs, the metal ions seemingly nucleate and grow at the edge-plane defective sites of GNs, therefore; the agglomerated GNs make a poor distribution of metal nanoparticles [26]. To solve this problem, functionalization of GNs with oxygen-containing groups is a useful method before using them as a support for metal nanoparticles.

In this work, treatment of pristine GNs was performed with a mixture of sulfuric acid and nitric acid for surface functionalization of GNs. After treatment of pristine GNs, a large amount of oxygen-containing groups, including carboxyl, hydroxyl, and carbonyl were produced on GNs. These groups could function as anchoring sites that improve the nucleation and deposition of the metal nanoparticles with smaller particle size and less aggregation.

Experimental

Reagents and apparatus

Palladium (II) chloride (PdCl_2), sulfuric acid (H_2SO_4), nitric acid (HNO_3) and potassium chloride (KCl) were purchased from Merck and used without further purification. High-purity nitrogen and oxygen gas were used in the experiments.

All electrochemical studies were performed using the potentiostat/galvanostat Autolab PGSTAT30 (Eco Chemie B.V., The Netherlands). The experiments were controlled by GPES 4.9 software in conjunction with a personal computer for data storage and processing. Experiments were carried out in a three-compartment cell containing a

modified glassy carbon electrode as working electrode, a platinum wire and a saturated calomel electrode (SCE) as counter and reference electrode, respectively. All electrodes were purchased from Azar electrode (Iran). All potentials in this work are referred to SCE.

Scanning electron microscopy images were obtained from a MIRA3 TESCAN made in Czech Republic. The XRD patterns of electrode surfaces were recorded on a X-ray diffractometer (D500 S) using Cu Ka ($k=1.54 \text{ \AA}$) radiation source (30–40 KV and 40–50 MA) in the range of $2\theta = 35\text{--}85^\circ$. All of the experiments were done at room temperature.

Functionalization of graphene nanosheets

Graphene nanosheets (carbon content > 99.5 wt%, diameter 1–20 μm , thickness 5–15 nm) was purchased from Xiamen Knano Graphit Technology Co. Graphene nanosheets was treated by sonicating in a mixture of concentrated sulfuric acid and nitric acid (1:1, v/v) for 2 h at 55 $^\circ\text{C}$ and then for 3 h at 80 $^\circ\text{C}$. Afterward, the nanosheets were washed with distilled water by filtration, repeating it several times until the pH of suspension reached nearly to 7.0. Finally, the graphene nanosheets were dried at room temperature for 24 h. During this process, the surface of graphene nanosheets was covered with carboxyl (–COOH), hydroxyl (–OH) and carbonyl (–C=O) groups.

Preparation of PdNPs modified GCE

Before the surface modification of GCE, the GC electrodes were polished to a mirror finish with alumina slurries. After alumina polishing, the electrodes were washed and ultrasonically cleaned in distilled water for 5 min and finally they were dried at room temperature in the air.

The working electrodes were modified using physical adsorption of suspension onto GCE substrate. A drop of dimethylformamide (DMF) suspension consisting of 5 mg/mL GNs or GO was dropped on top of the GCE. After solvent evaporation, palladium nanoparticles were deposited onto electrode surfaces using the electrochemical method.

A stock solution of PdCl_2 (5 mM) was prepared in 0.5 M H_2SO_4 . The resulting solution was stored at room temperature and in the dark. The palladium nanoparticles were synthesized by electrochemical reduction of 0.5 mM PdCl_2 in 0.5 M H_2SO_4 at a constant potential of 0.1 V for 60 s [27–28].

Results and discussion

Characterization of graphene and graphene oxide nanosheets

Figure 1 shows FT-IR spectra of graphene and graphene oxide. In spectrum of graphene oxide (b), the broad peak at 3400 cm^{-1} is relevant to the stretching vibrations of hydroxyl group. Peak at 1720 cm^{-1} corresponds to the stretching vibrations from carbonyl group. Peak at 1600 cm^{-1} corresponds to skeletal vibrations from non-oxide graphitic domains. Also the peak at 1220 and 1060 cm^{-1} corresponds to C–OH and C–O stretching vibrations, respectively [29].

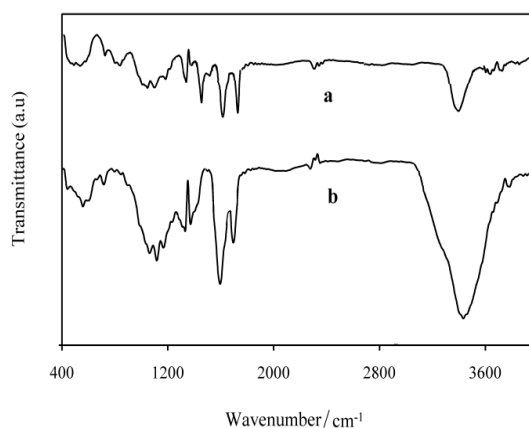


Figure 1. FT-IR spectra of (a) graphene and (b) graphene oxide

So, the presence of different type of oxygen-containing groups was confirmed in graphene oxide spectrum. The observed small peaks in graphene spectrum (a) are similar to graphene oxide because the graphene nanosheets has a few number of oxygen-containing groups.

Structural characterization

The surface morphology of the bare and modified GC electrodes was characterized by scanning electron microscopy. Figure 2a presents the morphology of the bare GCE surface after cleaning the process. As can be seen in this image, the bare GCE substrate is featureless. SEM image of GO/GCE in Figure 2b shows a typical wrinkled sheet texture of graphene. The

graphene oxide nanosheets with a large rough surface could provide a good scaffold for metal NPs depositing.

SEM images of dispersed PdNPs on GNs/GCE and GO/GCE are shown in Figure 2c-d, respectively. Comparison of these images clearly demonstrated that Pd spherical nanoparticles with particle size about 20 nm are totally uniform deposited on GO/GCE, but dispersed PdNPs on GNs/GCE have a fairly uniform distribution and larger particle size (about 40 nm).

It has been demonstrated that oxygen-containing groups could provide favorite nucleation sites for metal nanoparticles growth. They stabilize the nanoparticles by increasing nanoparticle-GO interaction [30].

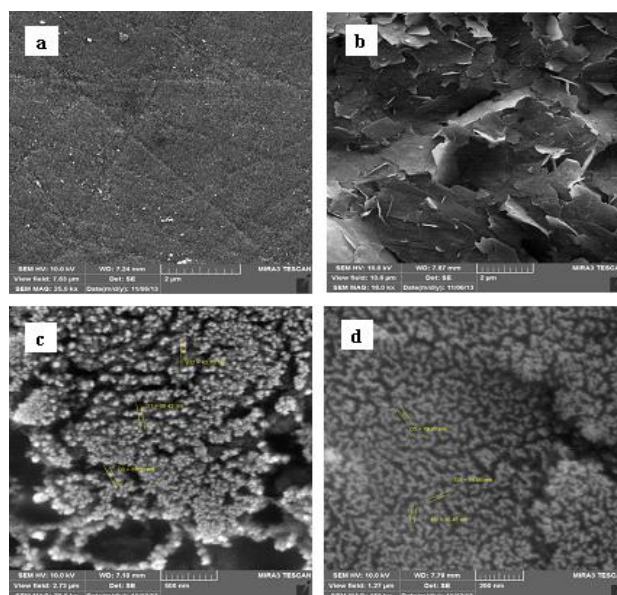


Figure 2. SEM images of (a) bare GCE, (b) GO/GCE, (c) PdNPs-GNs/GCE and (d) PdNPs-GO/GCE

Energy dispersive X-ray method was used to analyze the elemental composition of the PdNPs-GO/GC electrode surface (Figure 3A). The EDX spectrum displayed a strong peak at 0.28 keV and a weak peak at 0.5 keV corresponding to C K α and O K α , respectively. These peaks were attributed to the carbon atoms of graphene oxide nanosheets and oxygen atoms of oxygen-containing groups, respectively. Moreover, two prevalent peaks were observed at 2.83 and 3.00 keV corresponding to Pd L α_1 and Pd L α_2 , which confirming the presence of metallic Pd (from PdNPs) deposited on the electrode surface. The amount of

loaded Pd was about 86.76 wt. % of total weight. Furthermore, the successful synthesis of the Pd nanoparticles was confirmed by XRD analysis and the result is shown in Figure 3B. In the XRD pattern, the four diffraction peaks at corresponding values of 40.1, 45.7, 67.6 and 80.5 were observed that could be indexed to the (111), (200), (220) and (311) planes, respectively. The typical peaks of metallic Pd demonstrated that Pd has been decorated on the electrode surface in metallic state. Also, a sharp peak which was attributed to carbon from GO nanosheets was observed in value of 26.33.

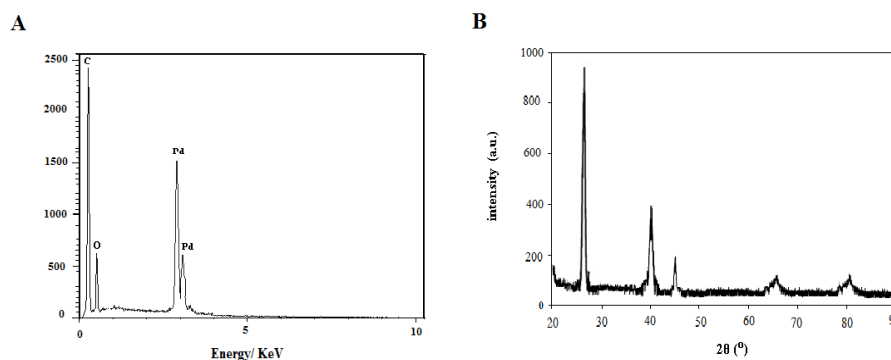


Figure 3. (A) EDX analysis and (B) X-ray diffraction pattern of PdNPs-GO modified GCE

The specific surface area of the bare and modified electrodes was calculated by CV method and $K_3Fe(CN)_6$ 1 mM solution was used as a probe at different scan rates (10 to 200 mV/s). For a reversible process, the following Randles-Sevcik equation (1) has being used.

$$I = 2.69 \times 10^5 A C^* n^{3/2} D^{1/2} v^{1/2} \quad (1)$$

where I refers to the peak current, n the electron transfer number, A the surface area of the electrode, D the diffusion coefficient, C^* the concentration of $K_3Fe(CN)_6$ and v is the scan rate.

This calculation showed that surface area of bare GCE, GNs/GCE and GO/GCE is 0.034, 0.12 and 0.14 cm^2 , respectively. The surface area of GNs/GCE and GO/GCE is higher than bare GCE.

Cyclic voltammetry study

After degassing H_2SO_4 solution by purging nitrogen gas for about 5 min, the cyclic voltammograms of bare and modified GC electrodes with GNs and GO were recorded. Under this condition, no reduction peak was appeared in the studied potential range for all three electrodes (Figure not shown).

Figure 4 illustrates cyclic voltammograms of the bare GCE (a) and the modified GC electrodes with

GNs (b) and GO (c) in O_2 -saturated 0.5 M H_2SO_4 solution at scan rate of 50 mV/s. In the oxygen saturated solution prepared by O_2 purging for 5 min, the reduction peaks were observed.

The obtained results revealed two important features of the modified electrodes. First, the reduction peak obviously appears for all three electrodes in the presence of oxygen. Peak current of ORR on the GNs/GCE and GO/GCE is higher than bare GCE, because GNs and GO act as a promoter for enhancing the electrochemical reaction. Also, they provide a large specific surface area and an increased heterogeneous electron transfer rate that plays an important role in the current enhancement.

Second, the onset potentials of O_2 -reduction on GNs/GC and GO/GC electrodes were remarkably shifted positively. It is a key parameter that reflects the catalytic activity of the catalyst. Oxygen reduction reaction occurs on the bare GCE at -0.15 V but on the GNs/GC and GO/GC electrodes take place at 0.10 V; indicating superior electrocatalytic activity of GNs and GO toward ORR. These results can be attributed to edge-plane sites of them, which provide many active sites for electron transfer [31].

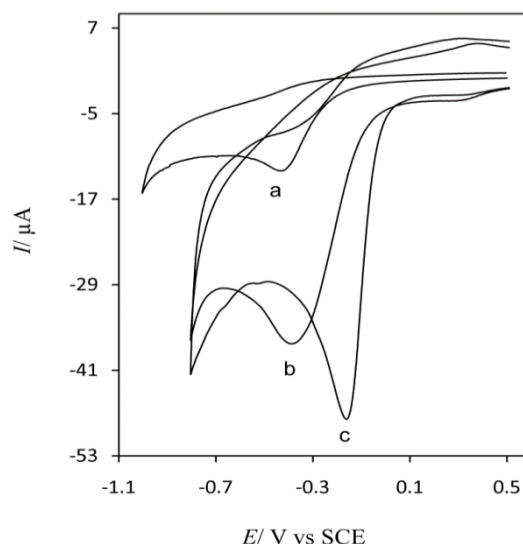


Figure 4. Cyclic voltammograms of (a) bare GCE, (b) GNs/GCE and (c) GO/GCE in O_2 -saturated 0.5 M H_2SO_4 solution at scan rate of 50 mV/s

Furthermore, as can be seen in Figure 4, GO/GCE not only increases the peak current more than GNs/GCE but also causes further shift of the peak potential in the positive direction. This behavior was demonstrated that functionalization of graphene nanosheets increases the density of edge-plane defective sites per mass and produces oxygen-containing groups at the edges or surface, which can increase the heterogeneous electron transfer rate.

The catalytic activity of the PdNPs/GC, PdNPs-GNs/GC and PdNPs-GO/GC electrodes toward ORR was evaluated by the cyclic voltammetry method in O_2 -saturated 0.5 mM H_2SO_4 (Figure 5).

In comparison with Figure 4, in the presence of palladium nanoparticles on the electrodes, oxygen-reduction potential was remarkably shifted anodically. It is obvious that Pd is the most effective catalyst for electrochemical reduction of oxygen. The catalytic peak currents of O_2 on

PdNPs-GNs/GCE and PdNPs-GO/GCE are much higher than that of PdNPs/GCE, which gives us a hint that GNs and GO increase specific surface area and the electrocatalytic activity of the electrode.

Also, the peak current of O_2 reduction on PdNPs-GO/GCE is larger than that of PdNPs-GNs/GCE, indicating that the loading of Pd on GO is more than GNs in same deposition conditions.

It should be noted that the cathodic current of oxygen reduction was overlapped with the reduction current of palladium oxide. Separating these two contributions accurately is impossible. However, the cathodic current of PdNPs-GO/GCE in N_2 -saturated solution confirms that the current of oxygen reduction in same conditions is much higher than that of palladium oxide reduction. Therefore, it can be concluded that the major contribution of the cathodic current in O_2 -saturated solution related to oxygen reduction.

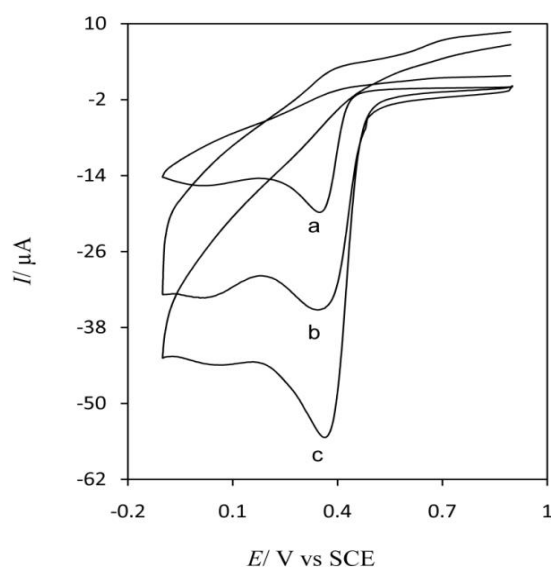


Figure 5. Cyclic voltammograms of (a) PdNPs/GCE, (b) PdNPs-GNs/GCE and (c) PdNPs-GO/GCE in O₂-saturated 0.5 mM H₂SO₄ at scan rate of 50 mV/s

Rotating disc electrode voltammetry study

The ORR kinetics was studied on GCE modified with PdNPs-GO using rotating disk electrode voltammetry method. The RDE voltammetry experiments were performed in O₂-saturated 0.5 M H₂SO₄ at various rotation rates from 100 to 800 rpm and at scan rate of 20 mV/s. The recorded

RDE voltammograms (Figure 6A) exhibited an increase in the current density with increase of the rotation rate, which is proportional to the square root of the rotation rate. The increased current density could be ascribed to decreasing of concentration polarization between electrolyte and electrode along with the increase of the electrode rotation rate.

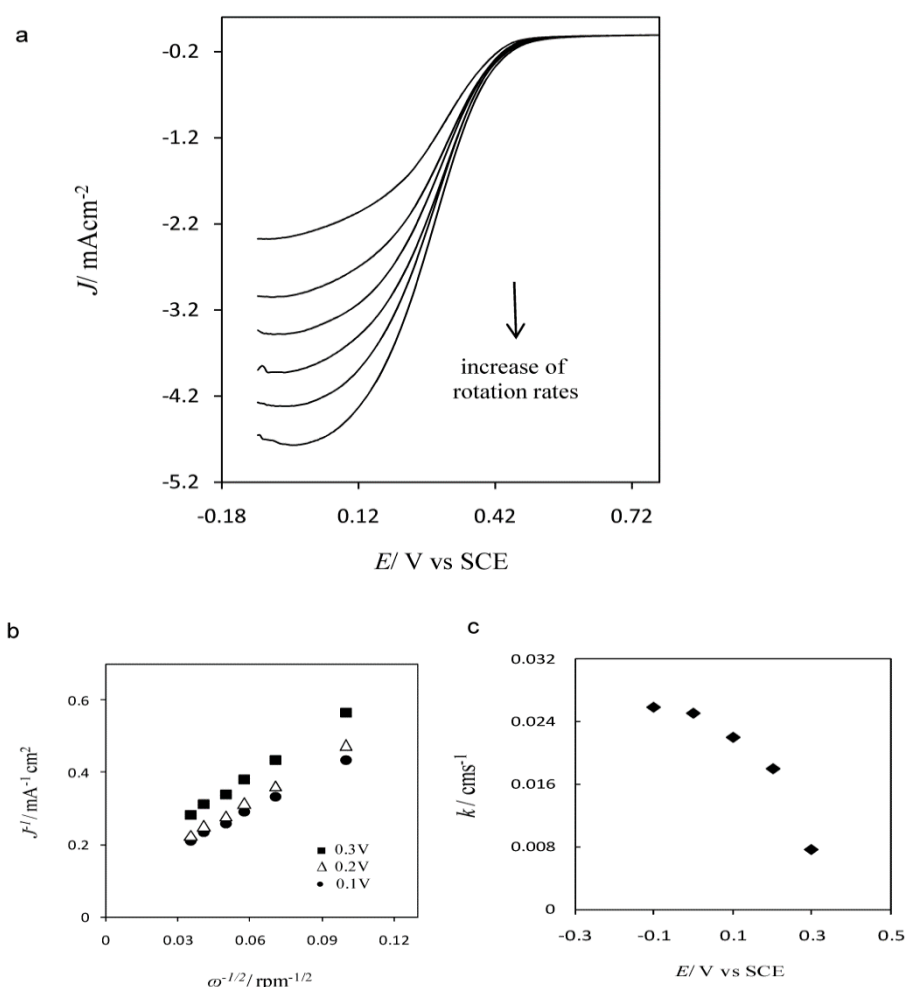


Figure 6. (A) LSVs of PdNPs-GO/GCE in O₂-saturated 0.5 mM H₂SO₄ at scan rate of 20 mV/s at different rotation rates (100, 200, 300, 400, 600 and 800 rpm) (B) Koutecky–Levich plot for O₂-reduction at different potentials (0.1, 0.2 and 0.3 V) (C) k_s values versus different potentials for ORR

The RDE voltammetry data were analyzed using the Koutecky-Levich plot ($1/J$ vs. $1/\omega^{1/2}$) at different potentials. The slopes of their best linear fit lines were used to compute the number of transferred electrons (n) based on the Koutecky-Levich equation (Eq. 2).

$$\frac{1}{j} = \frac{1}{j_k} + \frac{1}{j_d} = -\frac{1}{nFkC} - \frac{1}{0.62 nF v^{-1/6} D^{2/3} C \omega^{1/2}} \quad (2)$$

where j is the measured current density, j_k and j_d are the kinetic and diffusion-limited current densities, respectively, F

is the Faraday constant (96485 C/mol), ν is the kinematic viscosity of the solution (0.01 cm²/s), D is the diffusion coefficient of O₂ (1.4×10^{-5} cm²/s), C is the concentration of O₂ in the bulk solution (1.13×10^{-6} mol/cm³), k_s is the electron transfer rate constant and ω is the electrode rotation rate [32]. The current densities at various rotation rates in the potential range from 0.1 to 0.3 V were used to calculate the number of transferred electrons associated to ORR; then the reverse of current density ($1/J$) was plotted versus the reverse of square root of the rotation rate ($1/\omega^{1/2}$). Figure 6B shows the

corresponding Kouteckye-Levich plots. The non-zero value of the intercept expresses that the ORR is under the mixed kinetic-diffusion control in this region of potential. Based on Eq. (2), the number of transferred electrons in oxygen reduction was estimated to be 3.7, indicating the four-electron ORR on this noble metal.

Furthermore, the electron transfer rate constant (k_s) of O_2 -reduction on PdNPs-GO/GCE at different potentials was estimated using Kouteckye-Levich plot and Eq. (2) for a 4-electron process. The obtained k_s values showed an increase along with the decrease of potential (Figure 6C).

Scan rate study

In order to further investigation of the electrochemical behavior of oxygen reduction, the CVs were recorded at different potential scan rates over a range of 10-120 mV/s on PdNPs-GO/GCE in O_2 saturated 0.5 M H_2SO_4 . Figure 7 shows the obtained CVs; it can be seen that the peak currents increase along with the scan rate increasing. Also, the peak currents of first reduction wave linearly varied versus the square root of the scan rate (Inset of Figure 7). This fact demonstrates that the reduction of oxygen at PdNPs-GO/GCE is a diffusion-controlled process.

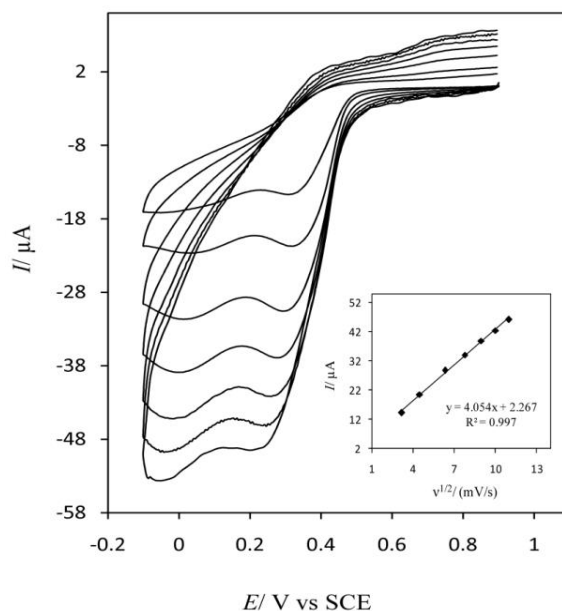


Figure 7. CVs of oxygen reduction on the PdNPs-GO/GCE in different scan rates in O_2 -saturated 0.5 mM H_2SO_4 . Inset: the plot of I_p versus $v^{1/2}$

For obtaining further information about the rate determining step of the ORR on PdNPs-GO/GCE, the Tafel plot was drawn using the equation (3) that is valid for a totally irreversible diffusion-controlled process:

$$E_p = b/2 \log v + \text{constant} \quad (3)$$

Where b indicates the cathodic Tafel slope ($b = 2.303RT/\alpha n_a F$). v , α and n_a

are the potential scan rate, the charge transfer coefficient and the electrons number involved in the rate determining step, respectively.

On the basis of Eq. (3), the slope of E_p versus $\log v$ plot was obtained 82.1 mV/decade, that this value is consistent with previous reports in the case of bulk palladium in acidic media [11]. Assuming a one-electron transfer

reaction in rate determining step, the charge transfer coefficient (α) was obtained as 0.36.

In addition, the value of n_a was calculated for the oxygen reduction on PdNPs-GO/GCE using the following equation [33].

$$|E_P - E_{P/2}| = 1.857RT/\alpha n_a F = 0.0477/\alpha n_a$$

$$\alpha n_a = \frac{0.0477}{|E_P - E_{P/2}|} \quad (4)$$

where $E_{P/2}$ is the potential corresponding to $I_{P/2}$. The value for αn_a was found to be 0.43 (assuming $n_a = 1$, hence $\alpha = 0.43$). It can be concluded that, there is a good agreement between the obtained α values from two ways.

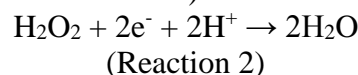
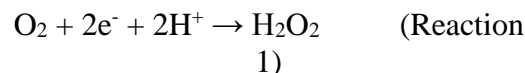
Possible mechanism of oxygen reduction on PdNPs-GO/GCE

As reported by Yeager [34], the oxygen reduction reaction usually proceeds through two main possible pathways. The molecular oxygen can be reduced directly to H_2O electrochemically (direct 4-electron reduction pathway) or the oxygen reduces to H_2O_2 , followed by a further reduction of H_2O_2 to H_2O (Two-step reduction pathway). The electrode material and the solution pH are efficient on mechanism of oxygen reduction. In this work, both of pathways were observed. As can be seen in Figure 4, cyclic voltammograms of all three electrodes in an O_2 -saturated solution show one reduction wave that is corresponding to the direct

four-electron pathway. This reaction for O_2 -reduction on carbon surfaces was cited by Yeager [34].



Cyclic voltammograms in Figure 8 shows typical CVs on the PdNPs-GO/GC electrode. Two reduction waves can be distinguished obviously; this fact implies that the oxygen reduction may proceed by a two-step pathway. The reduction of oxygen to H_2O_2 through a 2-electron reduction shows a peak that it observes at 0.32 V (Reaction 1) and the further reduction of electrogenerated H_2O_2 to H_2O exhibits the second weak peak at -0.05 V (Reaction 2).



Both of peak currents were enhanced after increasing the concentration of oxygen. The difference in the rate of electron transfer and in the rate of oxygen dissociation to adsorbed oxygen atoms leads to production of peroxide. The trapping of electrons by the oxygen atom on PdNPs-GO/GCE surface subsequently leads to the interaction of the negatively charged atoms with protons to form hydrogen peroxide.

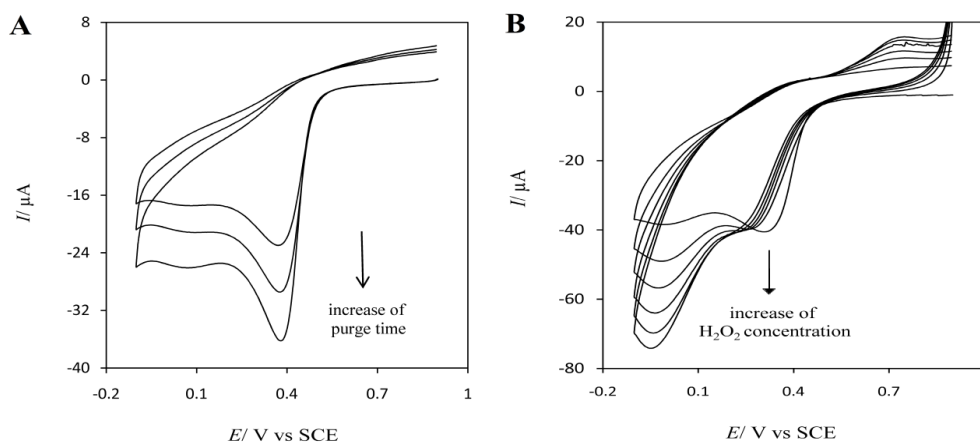


Figure 8. (A) CVs of PdNPs-GO/GCE in H_2SO_4 0.5 M with increase of purge time of O_2 (30, 60 and 90 s) (B) CVs of PdNPs-GO/GCE in H_2SO_4 0.5 M in the presence of O_2 and different concentrations of H_2O_2 (1, 2, 4, 6 and 8 mM) at scan rate of 50 mV/s

As illustrated in Figure 8A, both of peaks were increased along with the increase of purge time of O_2 into the electrolyte. But as shown in Figure 8B, when H_2O_2 was added into electrolyte, only second reduction peak was increased. This fact indicates that the second peak is according to the reduction of H_2O_2 . [33].

Stability study

Since durability is one of the essential concerns in fuel cell systems, the long-term durability for PdNPs/GCE, PdNPs-GNs/GCE and PdNPs-GO/GCE was investigated. Cyclic voltammograms (250 cycles) of these

electrodes were recorded in O_2 -saturated 0.5 mM H_2SO_4 (Figure 9). The PdNPs-GO/GCE exhibited superior performance in comparison with PdNPs/GCE and PdNPs-GNs/GCE in a long-term experiment.

The current density remained almost unchanged for PdNPs-GO/GCE and only a 0.8% drop in current density was detected while current density for PdNPs-GNs/GCE is reduced by 7% and for PdNPs/GCE by 17%. The oxygen containing groups play a main role in stabilizing PdNPs on graphene oxide nanosheets, therefore PdNPs-GO/GCE displayed high stability.

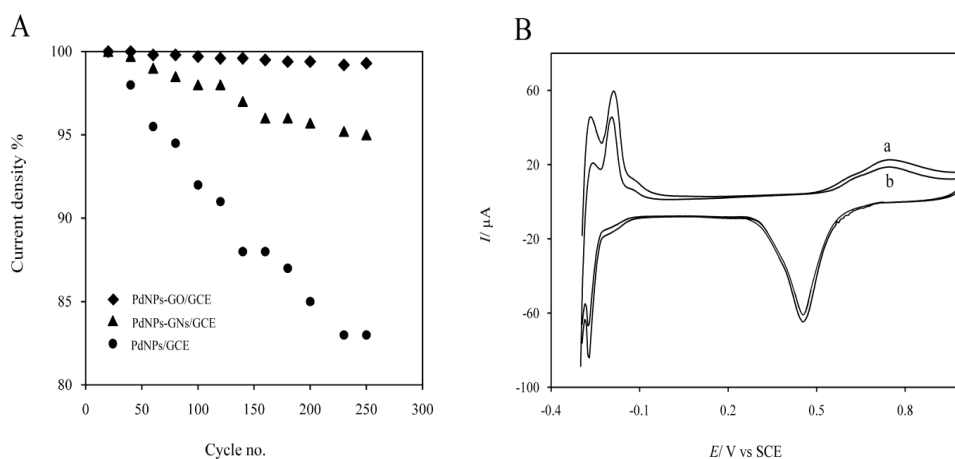


Figure 9. (A) Current density of electrodes vs. cycle no. (B) Cyclic voltammograms of PdNPs-GO/GCE a) before and b) after 250 cycles

Conclusion

The glassy carbon electrode modified with Pd nanoparticles supported by graphene oxide nanosheets was introduced. Pd nanoparticles with the small particle size and uniform distribution were prepared by electrodeposition method. The electro-reduction of oxygen on the proposed electrode has been studied and electrochemical experiments demonstrated that the PdNPs-GO has suitable electrocatalytic characteristics as a catalyst for the ORR. In a more detailed analysis, kinetic parameters were calculated by the Tafel analysis and the number of electrons for the ORR was found to be 3.7 by Kouteckye-Levich plot. Cyclic voltammetry measurements at different scan rates showed that ORR at the PdNPs-GO/GCE is a diffusion-controlled process. The investigation of activity and stability of PdNPs-GO/GCE demonstrated that this modified electrode is a desirable catalyst for ORR. Also, the graphene oxide nanosheets displayed superior performance compared to graphene nanosheets as a support for metal nanoparticles.

Acknowledgments

Financial support from the University of Tabriz is gratefully acknowledged.

References

- [1] N.M. Markovic, R.R. Adzic, B.D. Cahan, E.B. Yeager, *J. Electroanal. Chem.*, **1994**, 377, 249-254.
- [2] N. Le Bozec, C. Compère, M. L'Her, A. Laouenan, D. Costa, P. Marcus, *Corros. Sci.*, **2001**, 43, 765-786.
- [3] M. Stratmann, J. Müller, *Corros. Sci.*, **1994**, 36, 327-359.
- [4] I.T. Kim, M. Choi, H.K. Lee, J. Shim, *J. Ind. Eng. Chem.*, **2013**, 19, 813-818.
- [5] R. Carrera-Cerritos, V. Baglio, A.S. Aricò, J. Ledesma-García, M.F. Sgroi, D. Pullini, *Appl. Catal. B Environ.*, **2014**, 144, 554-560.
- [6] X. Ren, S.S. Zhang, D.T. Tran, J. Read, *J. Mater. Chem.*, **2011**, 21, 10118-10125.
- [7] C.O. Laoire, S. Mukerjee, K.M. Abraham, E.J. Plichta, M.A. Hendrickson, *J. Phys. Chem. C*, **2009**, 113, 20127-20134.
- [8] J. Bai, Q. Zhu, Z. Lv, H. Dong, J. Yu, L. Dong, *Int. J. Hydrogen Energy*, **2013**, 38, 1413-1418.
- [9] J.L. Fernández, D.A. Walsh, A.J. Bard, *J. Am. Chem. Soc.*, **2004**, 127, 357-365.
- [10] S-a. Jin, K. Kwon, C. Pak, H. Chang, *Catal. Today*, **2011**, 164, 176-180.
- [11] H. Erikson, M. Liik, A. Sarapuu, M. Marandi, V. Sammelselg, K. Tammeveski, *J. Electroanal. Chem.*, **2013**, 691, 35-41.
- [12] F. Fouda-Onana, S. Bah, O. Savadogo, *J. Electroanal. Chem.*, **2009**, 636, 1-9.
- [13] W. Sun, A. Hsu, R. Chen, *J. Power Sources*, **2011**, 196, 4491-4498.
- [14] H. Erikson, A. Sarapuu, K. Tammeveski, J. Solla-Gullón, J. M. Feliu, *Electrochem. Commun.*, **2011**, 13, 734-737
- [15] S. Chakraborty, C. Retna Raj, *Carbon*, **2010**, 48, 3242-3249.
- [16] J. Ustarroz, U. Gupta, A. Hubin, S. Bals, H. Terryn, *Electrochem. Commun.*, **2010**, 12, 1706-1709.
- [17] Z-L. Liu, R. Huang, Y-J. Deng, D-H. Chen, L. Huang, Y-R. Cai, *Electrochim. Acta*, **2013**, 112, 919-926.
- [18] H. Ji, M. Li, Y. Wang, F. Gao, *Electrochem. Commun.*, **2012**, 24, 17-20.

- [19] J. Li, H. Xie, L. Chen, *Sens. Actuators B*, **2011**, *153*, 239-245.
- [20] M.H. Seo, S.M. Choi, H.J. Kim, W.B. Kim, *Electrochem. Commun.*, **2011**, *13*, 182-185.
- [21] W. He, H. Jiang, Y. Zhou, S. Yang, X. Xue, Z. Zou, *Carbon*, **2012**, *50*, 265-274.
- [22] A.N. Golikand, M. Asgari, E. Lohrasbi, *Int. J. Hydrogen Energy*, **2011**, *36*, 13317-13324.
- [23] Y. Shao, J. Wang, H. Wu, J. Liu, IA. Aksay, Y. Lin, *Electroanalysis*, **2010**, *22*, 1027-1036.
- [24] T. Gan, S. Hu, *Microchim. Acta*, **2011**, *175*, 1-19.
- [25] E. Yoo, T. Okata, T. Akita, M. Kohyama, J. Nakamura, I. Honma, *Nano Lett.*, **2009**, *9*, 2255-2259.
- [26] M. Pumera, *Chem. Soc. Rev.*, **2010**, *39*, 4146-4157.
- [27] H. Ji, M. Li, Y. Wang, F. Gao, *Electrochem. Commun.*, **2012**, *24*, 17-20.
- [28] Z-L. Liu, R. Huang, Y-J. Deng, D-H. Chen, L. Huang, Y-R. Cai, Q. Wang, S-P. Chen, S-G. Sun, *Electrochim. Acta*, **2013**, *112*, 919-926.
- [29] D.R. Dreyer, S. Park, C.W. Bielawski, R.S. Ruoff, *Chem. Soc. Rev.*, **2010**, *39*, 228-240.
- [30] M. Pumera, A. Ambrosi, A. Bonanni, E.L.K. Chng, H.L. Poh, *Trends Analyt. Chem.*, **2010**, *29*, 954-965.
- [31] O.V. Prezhdo, P.V. Kamat, G.C. Schatz, *J. Phys. Chem. C*, **2011**, *115*, 3195-3197.
- [32] K. Tiido, N. Alexeyeva, M. Couillard, C. Bock, B.R. MacDougall, K. Tammeveski, *Electrochim. Acta*, **2013**, *107*, 509-517.
- [33] B. Habibi, M. Abazari, M.H. Pournaghi-Azar, *Colloids Surf. B*, **2014**, *114*, 89.
- [34] E. Yeager, *J. Mol. Catal.*, **1986**, *38*, 5-25.